

2

NAVAL POSTGRADUATE SCHOOL Monterey, California

AD-A240 587
[Barcode]

DTIC
ELECTE
SEP 13 1991
S D D



THESIS

PARAMETER IDENTIFICATION STUDIES
ON THE NASA/AMES RESEARCH CENTER
ADVANCED CONCEPTS FLIGHT SIMULATOR

by

Thomas P. McKavitt, Jr.

September, 1990

Thesis Advisor: Louis V. Schmidt

Approved for public release; distribution is unlimited.

01 9 12 073

91-10456
[Barcode]

REPORT DOCUMENTATION PAGE

1a. REPORT SECURITY CLASSIFICATION UNCLASSIFIED			1b. RESTRICTIVE MARKINGS			
2a. SECURITY CLASSIFICATION AUTHORITY			3. DISTRIBUTION/AVAILABILITY OF REPORT Approved for public release; distribution unlimited			
2b. DECLASSIFICATION/DOWNGRADING SCHEDULE						
4. PERFORMING ORGANIZATION REPORT NUMBER(S)			5. MONITORING ORGANIZATION REPORT NUMBER(S)			
6a. NAME OF PERFORMING ORGANIZATION Naval Postgraduate School		6b. OFFICE SYMBOL (If applicable) Code 51	7a. NAME OF MONITORING ORGANIZATION Naval Postgraduate School			
6c. ADDRESS (City, State, and ZIP Code) Monterey, CA 93943-5000			7b. ADDRESS (City, State, and ZIP Code) Monterey, CA 93943-5000			
8a. NAME OF FUNDING/SPONSORING ORGANIZATION		8b. OFFICE SYMBOL (If applicable)	9. PROCUREMENT INSTRUMENT IDENTIFICATION NUMBER			
8c. ADDRESS (City, State, and ZIP Code)			10. SOURCE OF FUNDING NUMBERS			
			PROGRAM ELEMENT NO	PROJECT NO	TASK NO	WORK UNIT ACCESSION NO
11. TITLE (Include Security Classification) PARAMETER IDENTIFICATION STUDIES ON THE NASA/AMES RESEARCH CENTER ADVANCED CONCEPTS FLIGHT SIMULATOR (UNCLASSIFIED)						
12. PERSONAL AUTHOR(S) McKavitt, Thomas P., Jr.						
13a. TYPE OF REPORT Engineer's Thesis		13b. TIME COVERED FROM _____ TO _____		14. DATE OF REPORT (Year, Month, Day) September 1990		
15. PAGE COUNT 73						
16. SUPPLEMENTARY NOTATION The views expressed in this thesis are those of the author and do not reflect the official policy or position of the Department of Defense or the U.S. Government.						
17. COSATI CODES			18. SUBJECT TERMS (Continue on reverse if necessary and identify by block number) Parameter identification, Aircraft simulator, Advanced Concepts Flight Simulator, ACFS			
FIELD	GROUP	SUB-GROUP				
19. ABSTRACT (Continue on reverse if necessary and identify by block number) The results of an aircraft parameter identification study conducted on the National Aeronautics and Space Administration/Ames Research Center Advanced Concepts Flight Simulator (ACFS) in conjunction with the Navy-NASA Joint Institute of Aeronautics are given. The ACFS is a commercial airline simulator with a design based on future technology. The simulator is used as a laboratory for human factors research and engineering as applied to the commercial airline industry. Parametric areas examined were engine pressure ratio (EPR), optimum long range cruise Mach number, flap reference speed, and critical take-off speeds. Results were compared with corresponding parameters of the Boeing 757 and 767 aircraft. This comparison identified two areas where improvements can be made: 1) low maximum lift coefficients (on the order of 20%-25% less than those of a 757; and 2) low optimum cruise Mach numbers. Recommendations were made to investigate certain software logic criteria in order to improve ACFS performance levels to those anticipated with the application of future technologies. Results of this study are applicable to future ACFS upgrades including a flight						
20. DISTRIBUTION/AVAILABILITY OF ABSTRACT <input checked="" type="checkbox"/> UNCLASSIFIED/UNLIMITED <input type="checkbox"/> SAME AS RPT <input type="checkbox"/> DTIC USERS			21. ABSTRACT SECURITY CLASSIFICATION Unclassified			
22a. NAME OF RESPONSIBLE INDIVIDUAL Louis V. Schmidt			22b. TELEPHONE (Include Area Code) (408) 646-2972		22c. OFFICE SYMBOL Code AA/Sc	

Unclassified

SECURITY CLASSIFICATION OF THIS PAGE

item 19 Continued: management system. These results are also tabulated for inclusion in the ACFS Performance Manual.

Approved for public release; distribution is unlimited.

Parameter Identification Studies
on the NASA/Ames Research Center
Advanced Concepts Flight Simulator

by

Thomas Patrick McKavitt, Jr.
Lieutenant, United States Navy
B.S., United States Naval Academy, 1983
M.S., Naval Postgraduate School, 1990

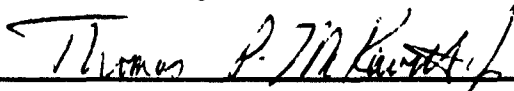
Submitted in partial fulfillment
of the requirements for the degree of

AERONAUTICAL AND ASTRONAUTICAL ENGINEER

from the

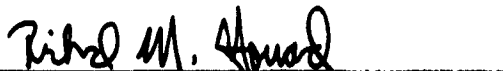
NAVAL POSTGRADUATE SCHOOL
September 1990

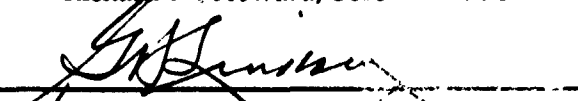
Author:

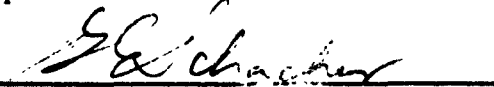

Thomas P. McKavitt, Jr.

Approved by:


Louis V. Schmidt, Thesis Advisor


Richard M. Howard, Second Reader


for E. Roberts Wood, Chairman
Department of Aeronautics and Astronautics


G. E. Schaefer
Dean of Faculty and Graduate Studies

ABSTRACT

The results of an aircraft parameter identification study conducted on the National Aeronautics and Space Administration/Ames Research Center Advanced Concepts Flight Simulator (ACFS) in conjunction with the Navy-NASA Joint Institute of Aeronautics are given. The ACFS is a commercial airline simulator with a design based on future technology. The simulator is used as a laboratory for human factors research and engineering as applied to the commercial airline industry. Parametric areas examined were engine pressure ratio (EPR), optimum long range cruise Mach number, flap reference speed, and critical take-off speeds. Results were compared with corresponding parameters of the Boeing 757 and 767 aircraft. This comparison identified two areas where improvements can be made: 1) low maximum lift coefficients (on the order of 20%-25% less than those of a 757); and 2) low optimum cruise Mach numbers. Recommendations were made to investigate certain software logic criteria in order to improve ACFS performance levels to those anticipated with the application of future technologies. Results of this study are applicable to future ACFS upgrades including a flight management system. These results are also tabulated for inclusion in the ACFS Performance

Manual.

Accession For	
NTIS CRA&I	<input checked="" type="checkbox"/>
DTIC TAB	<input type="checkbox"/>
Unannounced	<input type="checkbox"/>
Justification	
By	
Distribution/	
Availability Codes	
Dist	Avail and/or Special
A-1	



TABLE OF CONTENTS

I. INTRODUCTION	1
II. BACKGROUND	3
III. DETERMINATION OF MAXIMUM ENGINE PRESSURE RATIOS	9
A. THEORY	9
B. FLIGHT TEST PROCEDURES	13
1. Take-off	13
2. Climb	14
3. Go-around	16
C. FLIGHT TEST RESULTS	17
1. Take-off	17
2. Climb	17
3. Go-around	20
IV. DETERMINATION OF LONG RANGE CRUISE MACH NUMBERS	26
A. THEORY	26
B. FLIGHT TEST PROCEDURES	29

C.	FLIGHT TEST RESULTS	29
V.	DETERMINATION OF FLAP REFERENCE SPEEDS	32
A.	THEORY	32
B.	FLIGHT TEST PROCEDURES	34
C.	FLIGHT TEST RESULTS	35
VI.	DETERMINATION OF CRITICAL TAKE-OFF PARAMETERS	37
A.	THEORY	37
B.	FLIGHT TEST PROCEDURES	46
1.	Climb speed	46
2.	Airborne minimum control speed	46
3.	Decision speed/Balanced field length	46
C.	FLIGHT TEST RESULTS	47
VII.	CONCLUSIONS AND RECOMMENDATIONS	50
A.	CONCLUSIONS	50
B.	RECOMMENDATIONS	52
APPENDIX	53

LIST OF REFERENCES 57

INITIAL DISTRIBUTION LIST 58

LIST OF TABLES

TABLE III.1 Comparison of maximum take-off EPR (Part I)	18
TABLE III.2 Comparison of maximum take-off EPR (Part II)	19
TABLE III.3 Comparison of maximum climb EPR (Part I)	21
TABLE III.4 Comparison of maximum climb EPR (Part II)	22
TABLE III.5 Comparison of maximum climb EPR (Part III)	23
TABLE III.6 Comparison of maximum go-around EPR (Part I)	24
TABLE III.7 Comparison of maximum go-around EPR (Part II)	25
TABLE IV.1 Comparison of optimum long range cruise mach numbers and lift coefficients.	31
TABLE V.1 ACFS stall speeds	35
TABLE V.2 Comparison of flap reference speeds and maximum C_L	36
TABLE VI.1 ACFS balanced field length	48
TABLE VI.2 Comparison of critical take-off speeds	49
TABLE A.1 ACFS Take-off EPR	53
TABLE A.2 ACFS Climb EPR	54
TABLE A.3 ACFS Go-around EPR	55
TABLE A.4 ACFS Long range cruise Mach numbers	55
TABLE A.5 ACFS Critical take-off speeds	56

LIST OF FIGURES

Figure I.1 ACFS Design Comparison with Boeing 757 and 767	2
Figure II.1 ACFS aircraft model	5
Figure II.2 ACFS cockpit layout	7
Figure II.3 ACFS computer system	8
Figure III.1 Typical turbofan engine station designations	12
Figure VI.1 Take-off profiles	38
Figure VI.2 Take-off forces	40
Figure VI.3 Graphical determination of balanced field length and decision speed	45

LIST OF SYMBOLS

a	Acceleration (ft/s ²)
a	Local speed of sound (ft/s)
\bar{a}	Average acceleration (ft/s ²)
a_0	Standard sea level speed of sound (ft/s)
A	Area (ft ²)
ACAWS	Advisory, Caution and Warning System
ACFS	Advanced Concepts Flight Simulator
AEO	All Engines Operating
AGL	Above Ground Level
C	Celsius (temperature scale)
C_D	Drag coefficient
C_L	Lift coefficient
c.g.	Center of gravity
CRT	Cathode Ray Tube
d	Mathematical differential
D	Drag force (lb)
EOS	Experiment Operator's Station
EPR	Engine Pressure Ratio
F_g	Gross thrust force (lb)

F_n	Net thrust force (lb)
F_r	Ram drag force (lb)
FAR	Federal Aviation Regulations
FMS	Flight Management System
g	gravitational constant
GCA	Ground Controlled Approach
GCU	Global Common Utilities
Hg	Mercury
hr	hour
IMN	Indicated Mach Number
KCAS	Knots Calibrated Airspeed
L	Lift force (lb)
lb	Pound
LT	Lift Tailoring
m	Mass
\dot{m}	Mass flow rate (lb _m /s)
M	Mach number
M_{dd}	Drag divergence Mach number
MAC	Mean Aerodynamic Chord
MFD	Multi-Function Display
NASA	National Aeronautics and Space Administration
nm	Nautical mile

OAT	Outside Air Temperature ($^{\circ}\text{C}$)
OEI	One Engine Inoperative
p	Static pressure (lb/ft^2)
p_t	Stagnation pressure (lb/ft^2)
PLA	Power Lever Angle
q	Dynamic pressure (lb/ft^2)
R	Universal gas constant
R	Range
RPM	Revolutions Per Minute
s	Distance (ft)
S	Wing surface area (ft^2)
s_G	Ground roll distance (ft)
SFO	San Francisco International Airport
t	Time (s)
T	Temperature ($^{\circ}\text{C}$)
T	Thrust force (lb)
TAT	Total Air Temperature ($^{\circ}\text{C}$)
TSFC	Thrust Specific Fuel Consumption ($\text{lb}_{\text{fuel}}/\text{lb hr}$)
V_1	Decision speed (KCAS)
V_2	Climb speed (KCAS)
V_{∞}	Aircraft velocity (ft/s)
V_{EF}	Engine failure speed (KCAS)

V_j	Jet exhaust velocity (ft/s)
V_{mc_a}	Airborne minimum control speed (KCAS)
V_R	Rotation speed (KCAS)
V_{ref}	Reference speed (KCAS)
V_s	Stall speed (KCAS)
V_{sp}	Spoiler activation speed (KCAS)
V_w	Headwind velocity (KCAS)
V_x	Arbitrary velocity (KCAS)
W	Weight (lb)
W/S	Wing loading (lb/ft ²)
γ	Specific heat ratio
Δ	Mathematical difference
ϕ	Runway slope (rad)
μ	Friction coefficient
ρ	Local density (lb s ² /ft ⁴)
σ	Density ratio
θ	Absolute temperature ratio

ACKNOWLEDGMENTS

The author is indebted to the following individuals and groups who provided guidance, support and assistance throughout this research:

- Professor Louis V. Schmidt, Thesis Advisor, Naval Postgraduate School
- Mr. Bob Shiner, Director, Man-Vehicle Systems Research Facility, NASA/Ames Research Center
- Mr. Barry Sullivan, Manager, Advanced Concepts Flight Simulator, NASA/Ames Research Center
- Mr. Dave Peppitone, NSI Technology Services, Inc.
- Mr. Ramesh Panda, Sterling Software, Sterling Federal Systems, Inc.
- Mr. Chris Matthies, formerly of Sterling Software, Sterling Federal Systems, Inc.
- My wife and family

I. INTRODUCTION

The Advanced Concepts Flight Simulator (ACFS) of the Man-Vehicle Systems Research Facility located at the NASA/Ames Research Center is used to study the interaction of flight crews with their environment and each other. Experiments conducted at this facility aid in the design and implementation of cockpit devices and procedures. The realistic aircrew responses required to validate experimental results cannot be evoked if the crews do not believe they are taking part in an actual flight. The key to accurate simulator scenarios is the fidelity of the simulator itself. All phases of flight from pre-flight planning to engine shutdown must simulate real world conditions as much as possible. Therefore, critical take-off, cruise, and landing data must be available to the flight crew at all times as an aid to efficient decision making in terms of critical aircraft operating parameters. Since much of this data on the ACFS is presently untabulated a study was undertaken in association with the Navy-NASA Joint Institute of Aeronautics to determine certain performance characteristics. The areas of maximum engine pressure ratio (EPR), optimum long range cruise Mach numbers, flap reference speeds, and critical take-off velocities were designated as priority concerns and will be discussed in this report. The ACFS was designed to simulate a commercial transport employing futuristic technology and, as such, is under frequent revision. One future upgrade which served as the motivation behind this research is the inclusion of a Flight Management System (FMS). Results of this study will be applicable to FMS programming for several phases

of flight. Additionally, these results will be incorporated as appendices in future ACFS operations manuals. The author functioned as flight test engineer and test pilot, conducting approximately 150 flight hours of test flying over six months. Comparison of the data obtained from the ACFS was made with data contained in the Boeing 757 and 767 performance manuals (Ref. 1 and Ref. 2). Figure I.1 shows a comparison of the ACFS and the two Boeing aircraft in terms of size and payload parameters.

DESIGN PARAMETER	757	767	ACFS
WING SPAN (FT)	124.7	156.1	139.7
ASPECT RATIO	7.8	7.9	9.0
LENGTH (FT)	155.3	155.0	161.3
WING AREA (FT ²)	1994	3050	1994
WING SWEEP (°)	25.0	31.5	24.0
PASSENGERS (MAX)	186	290	200
MAX GROSS WEIGHT (LB)	220,000	350,000	220,000
TOTAL THRUST (LB)	74,800	113,500	83,700
FUEL LOAD (LB)	36,000	138,000	42,500

Figure I.1 ACFS Design Comparison with Boeing 757 and 767 (757 and 767 data from Ref. 3)

A performance analysis of the ACFS was completed previously by Major Paul F. Donohue, USMC [Ref. 3] and was consulted prior to initiating this study. This report represents the initial foray into cataloging the performance of the ACFS in terms of specific operating parameters at specific flight conditions. Follow on research will be continued through the Navy-NASA Joint Institute of Aeronautics in an effort to fully determine ACFS operating characteristics.

II. BACKGROUND

The need for more efficient information systems in every facet of life is well known and aviation systems are no exception. Systems which supply information to pilots and first officers of commercial airliners are critical to the safety of each flight. Designing accurate, easy to read instrumentation packages is a never ending process. Not only must a particular aircraft system be monitored in a specific way, but human factors engineers must consider how to arrange data displays to ensure proper interpretation. Constant improvements in avionics present a unique problem--as new systems are introduced and old systems retained as backups, how do engineers provide for both displays? Instead of simply adding more instruments to an already cluttered display panel, multi-function displays (MFDs) offer flexibility in information display and positioning. Quantum advances in computer technology lend themselves to just such an application. However, designing, installing and testing a "glass cockpit" is a lengthy and expensive proposition.

The development of a high fidelity flight simulator is a crucial link in the timely evaluation of cockpit display system concepts. The simulator allows for repeated tests using different flight crews under identical circumstances. In this way an objective evaluation of new systems can be made. The Advanced Concepts Flight Simulator (ACFS) was designed to meet this challenge head-on.

Using a technology base forecasted for the mid-1990's a design for a generic aircraft was created to fulfill the projected need for a 200-passenger, twin turbofan engine

transport with a 2500 nautical mile range and a cockpit crew of two. Predicted levels of technology led to the final design of a conventional planform, high aspect ratio wing; a digital fly-by-wire/light flight control system which uses all electric actuators; an electrically powered environmental control system; a light-weight composite structure; and a state-of-the-art desk-top style flight station [Ref. 5: p. 13-18]. Figure 1 shows the ACFS in three-view as a low-wing, T-tail configured aircraft with the engines mounted below each wing and a conventional tricycle landing gear. The heart of the simulator, however, is the cockpit station (Figure 2) the centerpiece of which is an arrangement of five multi-function displays. The two primary displays, situated in front of the captain and first officer, combine attitude and radar/navigation information. The three secondary displays have touch sensitive screens which permit aircrew to arrange system schematics, checklists, engine readouts, and caution/warning cues as desired. Each crewmember uses an outboard sidestick controller for pitch and roll rate inputs. Originally, two sets of interconnected dual throttles were in place; however recently, the communication/navigation frequency display and keypad were relocated to the center console and one set of dual throttles, accessible to both crewmembers, was placed in the center of the desk-top area. The ACFS is not motion capable as of this writing but a revision is in progress which will make the simulator fully motion capable in six degrees of freedom.

Any simulation environment is software intensive by nature and the ACFS is no exception. This study was conducted while the ACFS was configured with Upgrade II software. ACFS software is written in VAX FORTRAN 77, RATFOR, VAX C, and

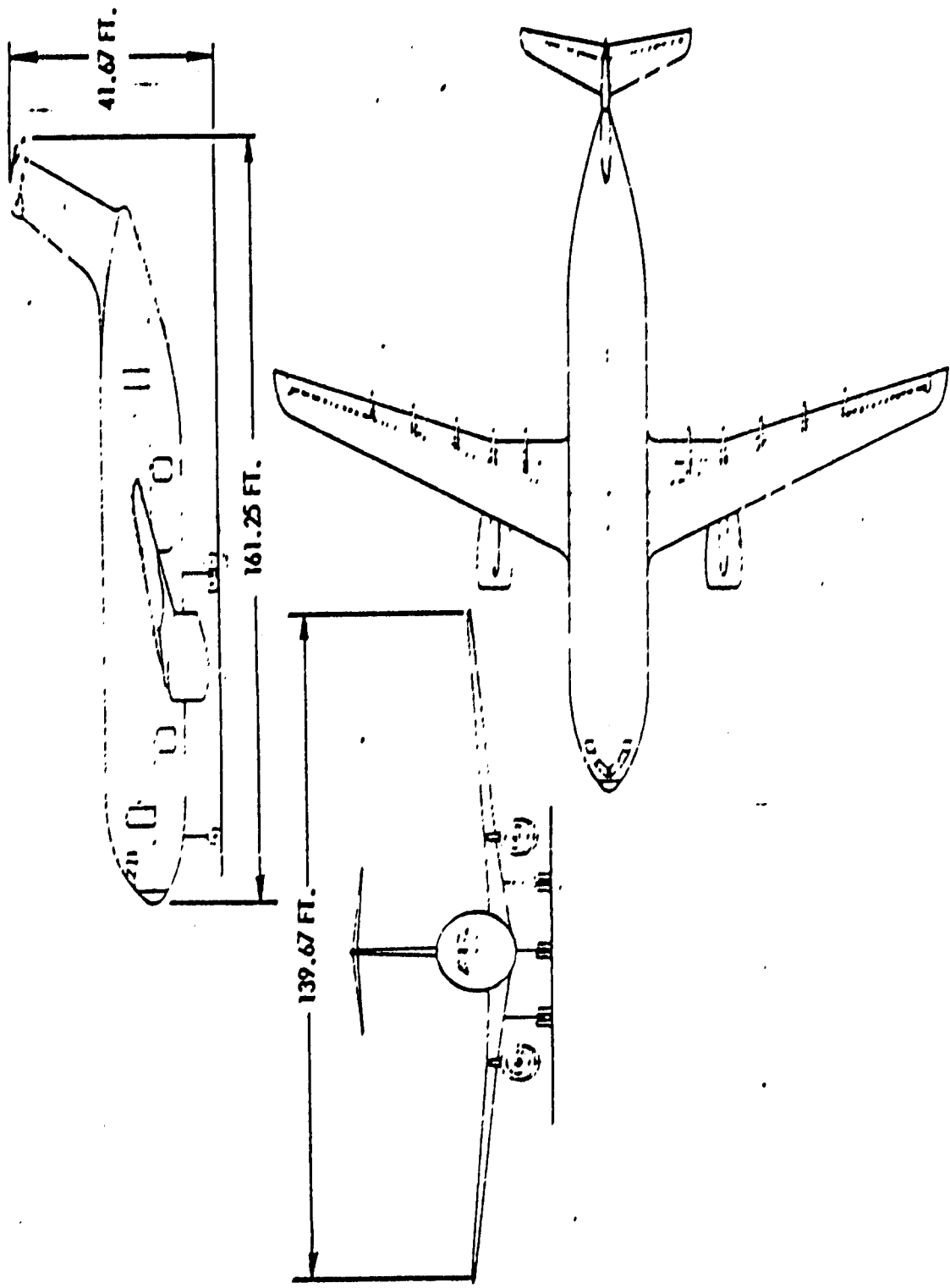
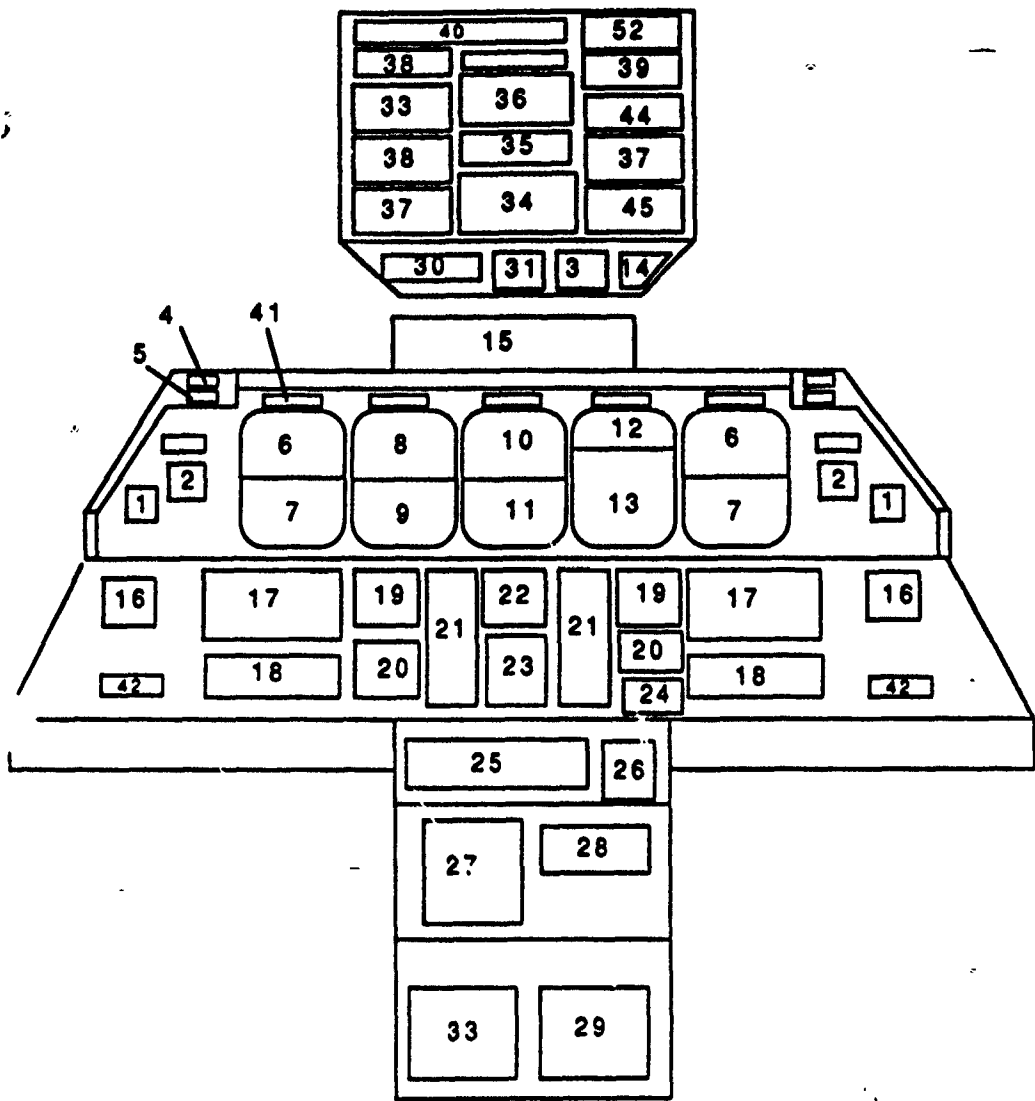


Figure II.1 ACFS aircraft model

VAX Macro Assembler computer languages [Ref. 6: p. 1-i]. The software is run by a VAX 8830 which uses VAX/VMS version 5.1 and interfaces with a VAX 6310 providing air traffic control simulation and four IRIS workstations which create the primary and secondary cockpit CRT displays, as shown in Figure 3. The VAX manages several different accounts for the ACFS system. In this way new designs can be debugged in the DEVELOPMENT account without affecting the actual software model. All test flights performed in the course of this research were conducted in the TEST account. Input/output interface with the VAX is accomplished through one of four experiment operator stations (EOS) one of which (station #1) is located inside the simulator cabin adjacent to the crew station. Throughout this study the EOS station #1 was used to display software variables by creating pages within the Global Common Utilities library for each flight regime examined. This enabled the simulator pilot to change or maintain certain flight parameters or conditions which were not displayed on the normal cockpit indicators. Magnetic tape was not used for data collection since it was not of a format compatible with computers at the Naval Postgraduate School. Therefore, data were recorded using the print screen function with a line printer connected to the EOS station. Any sort of time histogram was impractical due to the lack of a proper elapsed time variable in the ACFS computer system. Data reduction was accomplished by manually inputting data into various software routines for calculation and tabulation



- | | | | |
|-------------------------|---------------------------|---------------------------|-----------------------------|
| 1 Master Crt Brightness | 14 Fuel Quantity | 27.GPS Cntrl | 40 Fire Control Panel |
| 2 Clock | 15 GCP | 28 Radar | 41. CRT Alternate Source |
| 3 Wing Flap Indicator | 16 Sidestick | 29. Printer | 42 Park Brake Rudder Adjust |
| 4. Master Warning | 17 FMC/CDU | 30. Land Lights/ADX Wea | 43 Emer Gear Release |
| 5 Master Caution | 18 CDU Keys | 31. Gear | 44 Emer Circuit Breakers |
| 6 Flight Display | 19. NAV Display Cntrl | 32 FCS | 45 HUD |
| 7 Nav Display | 20 Transmit/Monitor Cntrl | 33 Eng Start | |
| 8 Engine Power/Status | 21. Throttles | 34. Gear/Brake Panel | |
| 9 CDWI/JEPP/Eng Status | 22 Freq Display | 35 Cabin ADV | |
| 10 ACAWS | 23 Freq Entry | 36 Interior Lights | |
| 11 CDTI | 24 ACARS | 37. APU/EXT Power | |
| 12 Checklists | 25 Alt Trim | 38 OXY/Emer Dep | |
| 13 System Schematics | 26 Wing Flap | 39 Cockpit Voice Recorder | |

Figure 11.2 ACFS cockpit layout

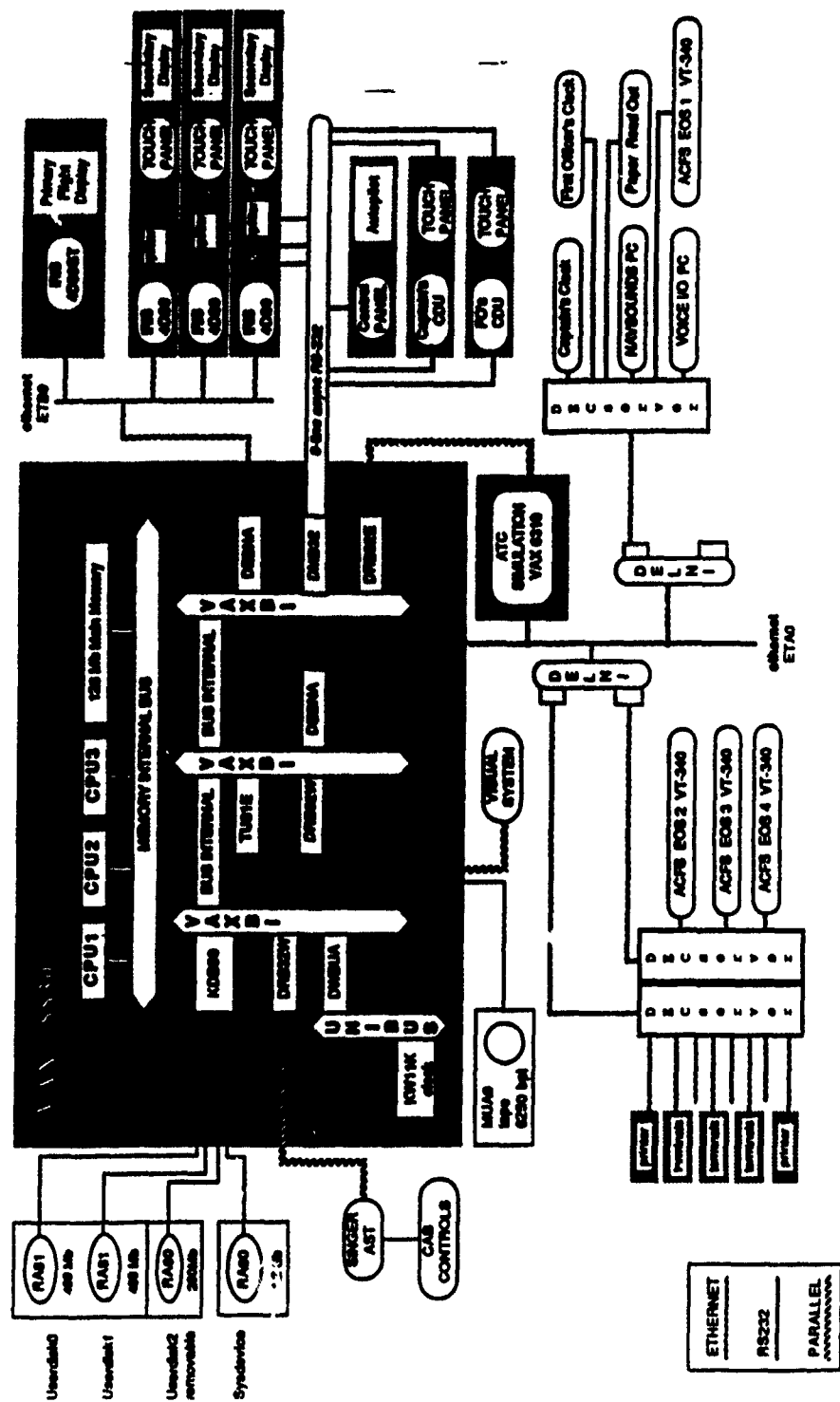


Figure II.3 ACFS computer system

III. DETERMINATION OF MAXIMUM ENGINE PRESSURE RATIOS

A. THEORY

Commercial transport aircrew operate their aircraft according to published guidelines and limitations which ensure safe and efficient handling. Power plants are the most critical mechanical system on any aircraft and, as such, require extremely close monitoring. Given the great expense associated with jet engines, their service life must be expended judiciously giving rise to engine operating limitations. These limitations can be expressed in terms of several different engine parameters such as fuel flow, low or high speed RPM, or engine pressure ratio (EPR).

Engine performance is commonly rated in terms of net thrust, F_n , as opposed to gross thrust. However, it is difficult and cost prohibitive to instrument engines for thrust readouts. Fortunately, other more easily monitored variables can be used as a measure of net thrust. For jet propulsion the net thrust results from a change in momentum of a control volume of air passing through the engine plus a pressure thrust which is the change in pressure of the air acting on the exhaust area. Starting with this definition an expression involving EPR can be derived. The contribution of the fuel to the total mass flow through the engine is assumed negligible as compared to the mass of air.

$$F_n = \dot{m} \Delta V + A_j(p_j - p_a) \quad (III.1)$$

where the subscripts j and a indicate jet exhaust and freestream conditions, respectively. For a jet exhaust which is fully expanded at the exit, $p_j = p_a$ and the pressure thrust term

vanishes. Using the continuity equation a substitution can be made for the mass flow term

$$\dot{m} = (\rho A V)_j = (\rho A V)_a \quad (\text{III.2})$$

The velocity change is

$$\Delta V = V_j - V_a \quad (\text{III.3})$$

where V_j is the exhaust jet velocity and V_a is the freestream or aircraft velocity. Substituting equations (III.2) and (III.3) into equation (III.1) results in

$$F_a = (\rho A V)_j V_j - (\rho A V)_a V_a \quad (\text{III.4})$$

The first term in this expression is known as the gross thrust, F_g , while the second term is the ram drag, F_r . Examining only the gross thrust term and substituting for V^2 gives

$$F_g = \rho A M^2 a^2 \quad (\text{III.5})$$

and assuming a perfect gas yields

$$\begin{aligned} \rho &= \frac{p}{gRT} \\ a &= \sqrt{\gamma gRT} \end{aligned} \quad (\text{III.6})$$

Now substituting equations (III.6) into equation (III.5) and simplifying gives

$$F_g = p A M^2 \gamma \quad (\text{III.7})$$

but p is static pressure and is related to total pressure by

$$p_t = p \left(1 + \frac{\gamma - 1}{2} M^2 \right)^{\frac{\gamma}{\gamma - 1}} \quad (\text{III.8})$$

This, in turn, can be substituted into equation (III.7) which yields

$$F_g = \frac{p_{t_7} A_7 M_7^2 \gamma}{\left(1 + \frac{\gamma - 1}{2} M_7^2 \right)^{\frac{\gamma}{\gamma - 1}}} \quad (\text{III.9})$$

where the subscript 7 indicates conditions at the jet exhaust nozzle as depicted in Figure III.1. A parallel development can be made for the ram drag term resulting in

$$F_r = \frac{p_{t_2} A_2 M_2^2 \gamma}{\left(1 + \frac{\gamma - 1}{2} M_2^2 \right)^{\frac{\gamma}{\gamma - 1}}} \quad (\text{III.10})$$

where the subscript 2 indicates conditions at the compressor face (Figure III.1). Recalling the definition of net thrust gives

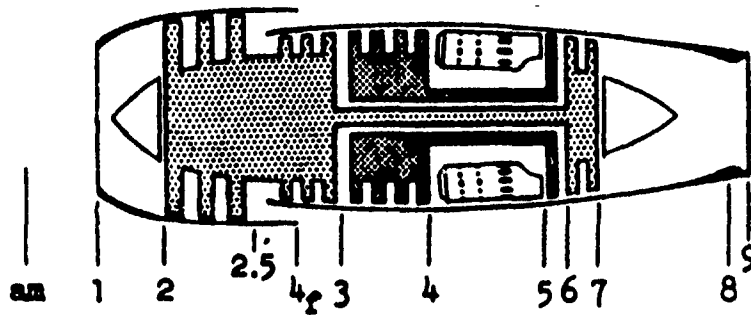


Figure III.1 Typical turbofan engine station designations

$$F_n = F_g - F_r$$

$$F_n = \frac{P_{t_7} A_7 M_7^2 \gamma_7}{\left(1 + \frac{\gamma-1}{2} M_7^2\right)^{\frac{\gamma}{\gamma-1}}} - \frac{P_{t_2} A_2 M_2^2 \gamma_2}{\left(1 + \frac{\gamma-1}{2} M_2^2\right)^{\frac{\gamma}{\gamma-1}}} \quad (\text{III.11})$$

and dividing through by P_{t_2} results in a final form of

$$\frac{F_n}{P_{t_2}} = \frac{P_{t_7}}{P_{t_2}} \frac{A_7 M_7^2 \gamma_7}{\left(1 + \frac{\gamma-1}{2} M_7^2\right)^{\frac{\gamma}{\gamma-1}}} - \frac{A_2 M_2^2 \gamma_2}{\left(1 + \frac{\gamma-1}{2} M_2^2\right)^{\frac{\gamma}{\gamma-1}}} \quad (\text{III.12})$$

The net thrust is now seen as a function of the ratio of total pressures at the exhaust nozzle and inlet or EPR. The use of EPR is favored since it takes into account any

changes in inlet conditions such as those experienced by aircraft operating over a wide range of altitudes.[Ref. 7: p. 2.13-2.15]

Maximum engine performance limitations are commonly set in terms of EPR for certain flight regimes such as take-off, climb, cruise, and go-around. The ACFS power plant model uses power lever angle (PLA) as an indication of the desired thrust setting and by virtue of this the maximum EPR values can be found by using maximum PLA for different flight conditions and varying pressure altitude.

B. FLIGHT TEST PROCEDURES

1. Take-off

The ACFS was positioned on the runway at San Francisco International Airport (SFO) with the parking brake applied to prevent aircraft movement once the throttles were advanced. Both throttles were advanced to 91.7% of full throttle throw, corresponding to maximum take-off PLA in the ACFS. Once the EPR readings had stabilized, the resulting EPR for each engine was recorded via hard copy of the GCU page created for the test. The following parameters were contained on the GCU page and monitored on EOS station #1:

- Pressure altitude
- Ambient temperature
- Engine pressure ratio (EPR)
- Computed power lever angle (PLA)
- Take-off power lever angle (PLA)

After EPR values for a particular temperature were recorded the ambient conditions were changed by selecting the EOS mode on the VAX computer. Throttle retardation was not necessary while changing ambient conditions since a constant position of 91.7% could be maintained. Once the full range of temperatures had been explored the pressure altitude was changed and the process repeated. Temperatures ranged from 10°C to 70°C and pressure altitude varied from sea level to 8000 feet.

2. Climb

The climb portion of the maximum EPR test conformed to a typical commercial transport climb profile, that is, flight in the clean configuration at 250 KCAS below 10,000 feet, then at 290 KCAS until intercepting 0.78 IMN [Ref. 1: p. 23.20.03]. An altimeter setting of 29.92" Hg was used in order to consistently fly pressure altitudes. Because the climb phase of flight is one of constant variation in altitude and temperature, a method for approximating climb conditions was necessary in order to obtain results applicable to particular altitude/temperature combinations. It was discovered that changing the outside air temperature (OAT) in order to change total air temperature (TAT) would result in a change in pressure altitude since no adjustment to the standard temperature lapse rate was possible. This occurrence made any attempt to match airspeed and TAT at one altitude while climbing extremely difficult. However, since EPR depends only on the ambient conditions and not on aircraft attitude, the same conditions could be reached while in level flight. Initially the ACFS was stabilized at the desired airspeed and altitude and OAT adjusted to modify TAT. This, in turn, altered the altitude.

Two iterations of this type were required to finally stabilize both altitude and TAT. With altitude, airspeed and TAT established the simulator was put in the FREEZE mode and both throttles advanced to a position of 77.3% of full throw position, corresponding to the ACFS climb PLA setting. The simulator was taken out of and put into FREEZE in less than two seconds in order to fine tune the throttle positions. This use of the FREEZE mode prevented large accelerations due to throttle advancement thus keeping TAT relatively constant. The ACFS was then taken out of FREEZE and allowed to accelerate until EPR was observed to stabilize on the engine instruments. The following parameters were monitored on EOS station #1:

- Pressure altitude
- Total temperature
- Engine pressure ratio
- Computed power lever angle (PLA)
- Maximum climb power lever angle (PLA)
- Indicated airspeed
- Indicated Mach number

These variables were recorded via hard copy of the EOS screen after EPR stabilization. The flight test spanned a TAT range of -20°C to 60°C. Test altitudes ranged from sea level to 40,000 feet.

3. Go-around

The go-around, or balked landing, phase of EPR testing was accomplished by flying multiple approaches to SFO while varying the airport OAT and pressure altitude. All approaches were flown in the landing configuration--landing gear down and flaps in the landing position (40° deflection). Height above ground level (AGL) was monitored on the ACFS radar altimeter. Upon reaching 200 feet AGL the simulator was put in the FREEZE mode and both throttles advanced to 95.5% corresponding to the emergency PLA position. By rapidly taking the simulator in and out of FREEZE, fine tuning of PLA was accomplished with only small altitude losses. The simulator was then taken out of FREEZE and allowed to descend to 100 feet AGL, a typical precision approach decision height, while the engines attained full power. The following parameters were stored in a GCU page and monitored on EOS station #1:

- Pressure altitude
- Outside air temperature (OAT)
- Engine pressure ratio (EPR)
- Computed power lever angle (PLA)
- Emergency power lever angle (PLA)
- Indicated airspeed

After stabilization the engine EPR values were recorded and a go-around initiated. The ACFS does not have the capability of airborne reinitialization; therefore the simulator was flown around the landing pattern in order to set up for subsequent approaches. By setting

the flaps to the take-off position (27°) and flying a modified ground controlled approach (GCA) pattern, the time required to transition from go-around to approach was reduced. Once the simulator was established on the downwind leg OAT was adjusted for the next approach. When a range of OATs had been tested the local altimeter was changed to effectively alter the elevation of SFO. A temperature range of 10°C to 55°C and an altitude range of sea level to 8000 feet was explored.

C. FLIGHT TEST RESULTS

1. Take-off

Tables III.1 and III.2 show the maximum take-off EPR values for the Boeing 757 and 767 aircraft and the ACFS as a function of airport OAT and pressure altitude. The trend of increasing EPR with both temperature and altitude in the case of the ACFS is consistent with both the 757 and 767. The general trend by aircraft type showed the 757 having the lowest EPR values followed by the 767. The ACFS consistently had the highest maximum EPR values throughout the range of altitudes and temperatures tested. None of the aircraft demonstrated any considerable change in maximum take-off EPR below temperatures of 20°C to 25°C.

2. Climb

Tables III.3-III.5 show a comparison of the ACFS maximum EPR settings for the climb phase of flight against those for the Boeing 757 and 767. The ACFS values follow the general trend of increasing with increasing altitude and decreasing temperature like the 757 and 767. However, the ACFS values exhibit different trends relative to the Boeing aircraft depending on altitude. At altitudes less than 10,000 feet the ACFS EPR values exceed those of the 757 while remaining lower than those of the 767. At 15,000 feet altitude the ACFS EPR values

TABLE III.1 Comparison of maximum take-off EPR (Part I)

OAT (°C)	AIRPORT PRESSURE ALTITUDE (FT)											
	SEA LEVEL			1000			2000			3000		
	AIRCRAFT TYPE											
	757	767	ACFS	757	767	ACFS	757	767	ACFS	757	767	ACFS
70	1.20	1.28	1.30	1.21	N	1.30	1.21	1.28	1.31	1.22	N	1.31
65	1.24	1.30	1.32	1.24	O	1.32	1.24	1.30	1.32	1.24	O	1.33
60	1.26	1.32	1.33	1.26	T	1.34	1.26	1.32	1.34	1.26	T	1.35
55	1.28	1.34	1.35	1.28		1.36	1.28	1.35	1.36	1.28		1.37
50	1.32	1.36	1.38	1.32	A	1.38	1.32	1.37	1.39	1.32	A	1.39
45	1.35	1.38	1.40	1.35	V	1.41	1.35	1.39	1.41	1.35	V	1.42
40	1.37	1.41	1.43	1.38	A	1.43	1.38	1.42	1.44	1.39	A	1.44
35	1.39	1.43	1.45	1.40	I	1.46	1.41	1.44	1.47	1.41	I	1.47
30	1.41	1.44	1.48	1.42	L	1.49	1.43	1.46	1.50	1.44	L	1.50
25	1.41	1.44	1.48	1.43	A	1.50	1.45	1.48	1.52	1.47	A	1.53
20	1.41	1.44	1.48	1.43	B	1.50	1.45	1.48	1.52	1.47	B	1.54
15	1.41	1.44	1.48	1.43	L	1.50	1.45	1.48	1.52	1.47	L	1.54
10	1.41	1.44	1.48	1.43	E	1.50	1.45	1.48	1.52	1.47	E	1.54

TABLE III.2 Comparison of maximum take-off EPR (Part II)

OAT (°C)	AIRPORT PRESSURE ALTITUDE (FT)											
	4000			5000			6000			8000		
	AIRCRAFT TYPE											
	757	767	ACFS	757	767	ACFS	757	767	ACFS	757	767	ACFS
70	1.22	1.29	1.31	1.23	N	1.32	1.23	1.29	1.32	1.23	1.29	1.32
65	1.24	1.31	1.33	1.24	O	1.34	1.24	1.31	1.34	1.24	1.31	1.34
60	1.26	1.33	1.35	1.26	T	1.36	1.26	1.33	1.36	1.26	1.33	1.36
55	1.28	1.36	1.37	1.28		1.38	1.28	1.36	1.38	1.28	1.35	1.38
50	1.32	1.38	1.40	1.32	A	1.40	1.32	1.38	1.40	1.32	1.38	1.40
45	1.35	1.40	1.42	1.35	V	1.43	1.35	1.40	1.43	1.35	1.40	1.43
40	1.39	1.43	1.45	1.39	A	1.46	1.39	1.43	1.46	1.39	1.43	1.45
35	1.42	1.45	1.48	1.43	I	1.49	1.43	1.46	1.48	1.43	1.46	1.48
30	1.45	1.47	1.51	1.45	L	1.52	1.45	1.48	1.52	1.45	1.49	1.51
25	1.48	1.49	1.54	1.49	A	1.55	1.49	1.50	1.55	1.49	1.51	1.55
20	1.49	1.50	1.56	1.51	B	1.58	1.52	1.53	1.58	1.52	1.53	1.58
15	1.49	1.50	1.56	1.51	L	1.58	1.53	1.53	1.60	1.55	1.56	1.62
10	1.49	1.50	1.56	1.51	E	1.58	1.53	1.53	1.60	1.56	1.56	1.63

exceed both Boeing aircraft although by only a slight margin in the case of the 767. For altitudes of 20,000 feet and above the ACFS exhibits higher EPR values than both aircraft at high temperatures and lower values at lower temperatures. Based on the assumption of advanced power plant technology in the 1995 time frame the EPR values would be expected to be consistently higher than both the 757 and 767.

3. Go-around

The maximum EPR values for the go-around flight phase are shown in Tables III.6 and III.7 for the ACFS and Boeing 757 and 767. The ACFS exhibits trends consistent with the two Boeing aircraft in terms of increasing altitude and temperature. Again, the ACFS demonstrates higher go-around EPR values throughout the test envelope which was expected.

TABLE III.3 Comparison of maximum climb EPR (Part I)

TAT (°C)	PRESSURE ALTITUDE								
	SEA LEVEL			5000			10000		
	AIRCRAFT TYPE								
	757	767	ACFS	757	767	ACFS	757	767	ACFS
60	1.15	1.20	1.19	1.14	1.19	1.17	1.12	1.17	1.16
50	1.18	1.24	1.23	1.17	1.22	1.22	1.16	1.21	1.20
40	1.22	1.28	1.26	1.21	1.27	1.25	1.19	1.25	1.24
30	1.24	1.31	1.28	1.25	1.32	1.30	1.23	1.31	1.28
20	1.24	1.31	1.28	1.27	1.35	1.33	1.28	1.37	1.34
10	1.24	1.31	1.28	1.27	1.35	1.33	1.30	1.39	1.37
0	1.24	1.31	1.28	1.27	1.35	1.33	1.30	1.39	1.37
-10	1.24	1.31	1.28	1.27	1.35	1.33	1.30	1.39	1.37
-20	1.24	1.31	1.28	1.27	1.35	1.33	1.30	1.39	1.37

TABLE III.4 Comparison of maximum climb EPR (Part II)

TAT (°C)	PRESSURE ALTITUDE								
	15000			20000			25000		
	AIRCRAFT TYPE								
	757	767	ACFS	757	767	ACFS	757	767	ACFS
60	1.08	1.13	1.15	1.05	1.12	1.16	1.02	1.11	1.15
50	1.11	1.17	1.19	1.09	1.16	1.19	1.06	1.15	1.17
40	1.15	1.22	1.23	1.13	1.21	1.22	1.11	1.20	1.21
30	1.20	1.28	1.28	1.18	1.27	1.27	1.16	1.27	1.26
20	1.25	1.34	1.35	1.23	1.34	1.33	1.21	1.34	1.32
10	1.29	1.39	1.39	1.29	1.41	1.39	1.27	1.41	1.39
0	1.29	1.39	1.39	1.32	1.45	1.43	1.35	1.50	1.48
-10	1.29	1.39	1.39	1.32	1.45	1.43	1.35	1.50	1.48
-20	1.29	1.39	1.39	1.32	1.45	1.43	1.35	1.50	1.48

TABLE III.5 Comparison of maximum climb EPR (Part III)

TAT (°C)	PRESSURE ALTITUDE (FT)								
	30000			35000			40000		
	AIRCRAFT TYPE								
	757	767	ACFS	757	767	ACFS	757	767	ACFS
60	0.99	1.08	1.19	0.98	1.07	****	0.97	1.06	****
50	1.04	1.13	1.22	1.03	1.11	1.19	1.02	1.10	****
40	1.09	1.18	1.22	1.08	1.17	1.21	1.07	1.16	****
30	1.14	1.25	1.23	1.13	1.23	1.24	1.12	1.23	1.26
20	1.19	1.32	1.29	1.18	1.31	1.31	1.18	1.30	1.30
10	1.26	1.40	1.37	1.25	1.39	1.37	1.24	1.38	1.36
0	1.33	1.48	1.45	1.32	1.47	1.43	1.32	1.46	1.44
-10	1.39	1.54	1.52	1.41	1.56	1.53	1.41	1.55	1.52
-20	1.39	1.54	1.52	1.48	1.58	1.61	1.50	1.58	1.61

**** NOT AVAILABLE

TABLE III.6 Comparison of maximum go-around EPR (Part I)

OAT (°C)	AIRPORT PRESSURE ALTITUDE (FT)															
	SEA LEVEL				1000				2000				3000			
	AIRCRAFT TYPE															
	757	767	ACFS	757	767	ACFS	757	767	ACFS	757	767	ACFS	757	767	ACFS	
55	1.27	1.32	1.35	1.27	N	1.35	1.27	1.33	1.36	1.27	1.33	1.36	1.27	N	1.38	
50	1.30	1.34	1.36	1.30	O	1.37	1.30	1.35	1.39	1.30	1.35	1.39	1.30	O	1.39	
45	1.33	1.36	1.39	1.33	T	1.40	1.33	1.37	1.41	1.33	1.37	1.41	1.33	T	1.42	
40	1.35	1.39	1.42	1.36		1.42	1.36	1.40	1.44	1.36	1.40	1.44	1.36		1.46	
35	1.37	1.41	1.44	1.38	A	1.46	1.39	1.42	1.47	1.39	1.42	1.47	1.39	A	1.49	
30	1.40	1.42	1.47	1.41	V	1.48	1.41	1.44	1.50	1.41	1.44	1.50	1.42	V	1.50	
25	1.40	1.42	1.47	1.42	A	1.50	1.43	1.46	1.53	1.43	1.46	1.53	1.45	A	1.55	
20	1.40	1.42	1.48	1.42	I	1.49	1.43	1.46	1.53	1.43	1.46	1.53	1.45	I	1.57	
15	1.40	1.42	1.48	1.42	L	1.49	1.43	1.46	1.53	1.43	1.46	1.53	1.45	L	1.55	
10	1.40	1.42	1.48	1.42		1.50	1.43	1.46	1.53	1.43	1.46	1.53	1.45		1.56	

TABLE III.7 Comparison of maximum go-around EPR (Part II)

OAT (°C)	AIRPORT PRESSURE ALTITUDE (FT)														
	4000				5000				6000				8000		
	AIRCRAFT TYPE														
	757	767	ACFS	757	767	ACFS	757	767	ACFS	757	767	ACFS	757	767	ACFS
55	1.27	****	1.37	1.27	N	1.38	1.27	****	1.38	1.27	****	1.38	1.27	****	1.38
50	1.30	1.35	1.40	1.29	O	1.40	1.29	1.36	1.40	1.29	1.36	1.40	1.29	****	1.40
45	1.33	1.38	1.42	1.33	T	1.44	1.33	1.38	1.43	1.33	1.38	1.43	1.33	1.38	1.43
40	1.36	1.41	1.45	1.36		1.46	1.36	1.41	1.46	1.36	1.41	1.46	1.36	1.41	1.46
35	1.40	1.43	1.49	1.40	A	1.49	1.40	1.44	1.48	1.40	1.44	1.48	1.40	1.44	1.48
30	1.43	1.45	1.52	1.43	V	1.53	1.43	1.46	1.53	1.43	1.46	1.53	1.43	1.47	1.53
25	1.46	1.47	1.54	1.46	A	1.56	1.46	1.49	1.57	1.46	1.49	1.57	1.46	1.49	1.56
20	1.47	1.48	1.57	1.49	I	1.60	1.50	1.51	1.60	1.49	1.51	1.60	1.49	1.51	1.60
15	1.47	1.48	1.57	1.49	L	1.60	1.51	1.52	1.62	1.51	1.52	1.62	1.52	1.54	1.63
10	1.47	1.48	1.58	1.49		1.60	1.51	1.52	1.62	1.51	1.52	1.62	1.53	1.54	1.65

**** NOT AVAILABLE

IV. DETERMINATION OF LONG RANGE CRUISE MACH NUMBERS

A. THEORY

Economy is paramount to the success of any commercial air carrier and the single greatest contributor is aircraft fuel efficiency. A discussion of aircraft range is actually a discussion of the fuel efficiency of a given aircraft, that is, optimizing distance traveled for fuel consumed. This relation is the first step in developing a range equation, thus

$$\frac{\text{distance}}{\text{lb}_{\text{fuel}}} = - \frac{dR}{dW} \quad (\text{IV.1})$$

The negative sign accounts for the weight lost as fuel is burned. The left side of equation (IV.1) can be defined as

$$\frac{\text{distance}}{\text{lb}_{\text{fuel}}} = \frac{\text{distance}}{\text{hr}} \frac{\text{hr}}{\text{lb}_{\text{fuel}}} \quad (\text{IV.2})$$

Letting distance become nautical miles and rearranging the second term gives

$$\frac{\text{nm}}{\text{lb}_{\text{fuel}}} = \frac{\text{nm}}{\text{hr}} \frac{1}{\frac{\text{lb}_{\text{fuel}}}{\text{hr}}} \quad (\text{IV.3})$$

The second term is recognized as the inverse of fuel flow. The definition of thrust specific fuel consumption (TSFC) proves useful here.

$$\text{TSFC} = \frac{\text{lb}_{\text{fuel}}}{\text{hr}} \quad (\text{IV.4})$$

$$(\text{T})\text{TSFC} = \frac{\text{lb}_{\text{fuel}}}{\text{hr}}$$

Substituting equations (IV.3) and (IV.4) into equation (IV.2) results in

$$\frac{\text{nm}}{\text{lb}_{\text{fuel}}} = \frac{V}{(\text{T})\text{TSFC}} \quad (\text{IV.5})$$

Remembering that in level, unaccelerated flight, or cruise at a constant airspeed, thrust is equal to drag and lift is equal to weight then equation (IV.5) becomes

$$\frac{\text{nm}}{\text{lb}_{\text{fuel}}} = \frac{V}{\text{TSFC}} \frac{L}{D} \frac{1}{W} \quad (\text{IV.6})$$

Airspeed at any arbitrary altitude can be related to Mach number through

$$V = a_0 \sqrt{\theta} M \quad (\text{IV.7})$$

where a_0 is the sea level standard day speed of sound and θ is the ratio of absolute temperature at altitude to that at standard day sea level. Substituting these relationships into equation (IV.6) gives

$$\frac{nm}{lb_{fuel}} = \frac{a_0 \sqrt{\theta}}{TSFC} M \frac{L}{D} \frac{1}{W} \quad (IV.8)$$

Now substituting equation (IV.8) into equation (IV.1) and solving for dR yields

$$dR = - \frac{a_0 \sqrt{\theta}}{TSFC} M \frac{L}{D} \frac{dW}{W} \quad (IV.9)$$

For a given altitude and assuming, again, level unaccelerated flight, all terms in equation (IV.9) except weight and TSFC are constant. However, it is known that in the cruise phase of flight TSFC varies very little with changes in Mach number and will be assumed to remain constant. Thus only the weight terms remain inside the integral

$$R = - \frac{a_0 \sqrt{\theta}}{TSFC} M \frac{L}{D} \int_{W_1}^{W_2} \frac{dW}{W} \quad (IV.10)$$

or,

$$R = - \frac{a_0 \sqrt{\theta}}{TSFC} M \frac{C_L}{C_D} \ln \frac{W_1}{W_2} \quad (IV.11)$$

It is now seen that range can be maximized at any altitude and gross weight by flying such that the product $M(C_L/C_D)$ is a maximum. [Ref. 7: p. 3.116-3.118]

B. FLIGHT TEST PROCEDURES

The range factor $M(C_L/C_D)$ is not an ACFS system variable but was created using a spare variable in order to be displayed on a GCU variable page. The ACFS was established in level flight at a desired altitude and gross weight at approximately 0.60 to 0.65 IMN. Gross weight was kept constant by using the fuel freeze function available in the VAX EOS menu. Mach number was then increased by adding power while maintaining altitude and monitoring the range factor variable until a maximum was achieved. The following parameters were included in the GCU page:

- Pressure altitude
- Lift coefficient
- Drag coefficient
- Gross weight
- Mach number
- Range parameter

When the range parameter was maximized these variables were recorded via hard copy of the GCU page. Gross weight was varied from 160,000 to 200,000 pounds at altitudes from 25,000 to 40,000 feet.

C. FLIGHT TEST RESULTS

Table IV.1 is a matrix of optimum long range cruise Mach numbers and lift coefficients for the ACFS and Boeing 757 and 767. The ACFS conformed to the

expected trend of increasing optimum cruise Mach number with increasing altitude. The lightest gross weight for which 767 data was available corresponded to the heaviest gross weight used in this test. The turbojet engines developed for a weight range as different as this would expectedly result in lower cruise Mach numbers for the same weight. For these reasons comparison with the 767 yielded limited information. However, the optimum cruise Mach numbers overall were lower than those of the 757. Initially, this was believed to be a result of a premature occurrence of drag divergence. However, after further examination of the test data, no indications of drag divergence were found.

Attention was then shifted to the effect of wing loading (W/S). The ACFS wing loading is approximately 10% less than that of the 757. Taking the optimum cruise Mach numbers for the ACFS and the Boeing aircraft at their respective altitudes, lift coefficients can be determined for all cases. The lower optimum cruise Mach numbers in the case of the ACFS were then qualified since the ACFS lift coefficients were as high if not higher than those of the 757. The inverse relationship between Mach number and C_L is apparent although the magnitudes are small. If drag coefficients had been known for the 757, relative trade-offs between Mach, C_L and C_D could have been examined to further qualify the results.

TABLE IV.1 Comparison of optimum long range cruise mach numbers and lift coefficients.

GROSS WEIGHT (LB)	ALTITUDE (FT)					
	25000			30000		
	AIRCRAFT TYPE					
	757	767	ACFS	757	767	ACFS
200000	0.70	0.61	0.66	0.75	0.66	0.71
	0.37	0.32	0.39	0.40	0.34	0.41
180000	0.66	****	0.66	0.73	****	0.69
	0.38		0.35	0.38		0.40
160000	0.63	****	0.60	0.69	****	0.65
	0.37		0.38	0.38		0.40
GROSS WEIGHT (LB)	ALTITUDE (FT)					
	35000			40000		
	AIRCRAFT TYPE					
	757	767	ACFS	757	767	ACFS
200000	0.77	0.73	0.73	0.80	0.78	0.75
	0.48	0.35	0.50	0.57	0.38	0.58
180000	0.74	****	0.72	0.80	****	0.74
	0.47		0.46	0.51		0.54
160000	0.71	****	0.71	0.80	****	0.72
	0.46		0.41	0.46		0.51

**** NOT AVAILABLE

V. DETERMINATION OF FLAP REFERENCE SPEEDS

A. THEORY

The most critical stages of any flight are take-off and landing. To allow for flight at slower speeds during these evolutions aircraft employ high lift devices such as flaps and slats which alter the camber and surface of a wing. However, deploying these movable surfaces into the airstream is not without penalty--aircraft drag and pitching moments are drastically affected. A range of flap settings is desirable so that just enough high lift augmentation is used. For example, in the landing phase not only is it desirable to have more precise control but low airspeeds as well. The take-off phase does not require as much lift augmentation since the aircraft is accelerating continuously. The ACFS has a four position flap/slat system:

- Clean--flaps and slats retracted
- Lift Tailoring (LT)--flaps 5°, slats fully extended
- Take-off--flaps 27°, slats fully extended
- Land--flaps 40°, slats fully extended

Commercial airline crews conform to certain procedural guidelines concerning minimum airspeed in all aircraft configurations to avoid stalls. Normally this consists of marking with a "bug" on the airspeed indicator a minimum reference speed commensurate with the aircraft configuration. A reference of this nature simplifies other procedures such

as flap retraction schedules by using criteria such as "bug plus 20 knots", for instance. Reference speed is defined by Federal Aviation Regulations (FAR) Part 25 as 30% higher than stall speed for any given configuration, or

$$V_{\text{ref}} = 1.30 V_s \quad (\text{V.1})$$

This leads into a discussion of the determination of stall speed.

Aircraft stalls occur when further increases in angle of attack no longer result in increases in lift. The aerodynamic mechanism of lift production is complex since influences such as maneuvering dynamics, turbulence and elastic deformations of the structure can all affect the onset of stall.

Subjecting an aircraft to a stall series test is straightforward and has few restrictions provided the subject aircraft has controllable post-stall characteristics. The four major requirements for a valid stall analysis are:

- Center of gravity (c.g.) in the most adverse position
- Idle thrust
- Deceleration rates of less than 1 knot per second
- Constant 1 'g' flight [Ref. 7: p. 3.32-3.33]

In demonstrating stall for certification purposes the aircraft flight path actually becomes somewhat curvilinear due to the loss in altitude subsequent to stall onset. Although 1 'g' flight is assumed, the actual flight dynamics show that vertical acceleration is on the order of 0.9 'g'. The actual value depends on factors such as c.g.

the actual deceleration rate induced by the pilot. For this reason any lift coefficients calculated from stall data in this manner must be corrected to 1 'g'.

B. FLIGHT TEST PROCEDURES

The ACFS stall series incorporated approaches to stall in all four flap configurations for gross weights of 150,000 to 200,000 pounds in 10,000 pound increments. The center of gravity of the aircraft was moved to the forward limit of 21% mean aerodynamic chord (MAC). Stalls were conducted at 5000 feet and stall speed was recorded in terms of calibrated airspeed. The use of calibrated airspeed served two purposes. First, it put stall speed in the same reference which a pilot uses. Secondly, the need for adjustments due to temperature and altitude considerations was eliminated.

The simulator was stabilized on altitude at close to minimum flying speed and the throttles retarded to establish a deceleration rate of not more than one knot per second. Altitude was maintained by applying backstick pressure and the Advisory, Caution and Warning System (ACAWS) display monitored for stall indications. Once a stall was indicated on the ACAWS display the simulator was put into the FREEZE mode and data recorded. The following parameters were stored in the stall GCU page:

- Pressure altitude
- Calibrated airspeed
- Gross weight
- Center of gravity (c.g.) location
- Z-axis acceleration of the center of gravity

C. FLIGHT TEST RESULTS

Table V.1 shows the ACFS stall speeds in calibrated airspeed and the maximum lift coefficients for the clean configuration. The proper correspondence of increasing stall speed with increasing weight was exhibited and C_L is seen to be relatively constant, which was expected. Table V.2 is a comparison of reference speeds corresponding to various flap settings of the ACFS and Boeing 757 and 767. The differences in gross weight ranges and standard flap settings between the three aircraft made comparison somewhat difficult. However, in comparing the 757 at 25° flap deflection and the ACFS at 27° flap deflection the ACFS was found to require a minimum of approximately ten knots additional airspeed to avoid stalling. Recalling the previous discussion involving wing loading from Chapter IV, it was suspected this increase in required airspeed was due to a lower maximum C_L in the ACFS since the simulator wing loading is less than that of the 757. As seen in Figure V.2 maximum lift coefficient values for the ACFS using 27° of flaps are between 20% and 25% lower than those for the 757 with a 25° flap setting.

TABLE V.1 ACFS stall speeds

WEIGHT (1000 LB)	150	160	170	180	190	200	210	220
V_s (KCAS)	152	155	160	167	169	174	178	182
C_L max	1.03	1.05	1.05	1.02	1.05	1.04	1.05	1.05

TABLE V.2 Comparison of flap reference speeds and maximum C_L

GROSS WEIGHT (1000 LB)	757 AIRCRAFT		
	FLAPS		
	30°	25°	20°
240	148/2.74	150/2.67	158/2.41
220	140/2.81	142/2.73	151/2.41
200	133/2.83	135/2.75	144/2.41
180	125/2.88	127/2.79	136/2.44
160	117/2.93	119/2.83	128/2.44
140	109/2.95	111/2.84	119/2.47
GROSS WEIGHT (1000 LB)	767 AIRCRAFT		
	FLAPS		
	30°	25°	20°
200	116/2.43	119/2.31	123/2.16
GROSS WEIGHT (1000 LB)	ACFS AIRCRAFT		
	FLAPS		
	40°	27°	5°
220	137/2.71	156/2.09	191/1.36
210	132/2.77	150/2.15	188/1.36
200	130/2.74	146/2.16	186/1.34
190	128/2.68	144/2.10	180/1.35
180	124/2.70	138/2.19	175/1.35
170	121/2.68	135/2.13	171/1.33
160	116/2.72	132/2.12	164/1.37
150	115/2.61	127/2.15	159/1.39

VI. DETERMINATION OF CRITICAL TAKE-OFF PARAMETERS

A. THEORY

Given the wide range of take-off conditions a commercial airline crew faces including gross weight, air temperature, pressure altitude, field length, wind, and runway slope the distance required to accelerate to lift-off speed and clear a 35 foot obstacle or accelerate, abort and come to rest on the runway may vary greatly. This section of testing deals with the calculation of V_1 , the decision speed, and balanced field length.

The take-off phase is characterized by several unique speeds which are defined as follows. Engine failure speed, V_{EF} , is the point at which the one-engine-inoperative (OEI) case begins. Decision speed, V_1 , is the point at which the pilot recognizes engine failure and decides to continue or abort the take-off. Rotation speed, V_R , is the point at which rotation to the take-off attitude is commenced and will be taken as

$$V_R = 1.05 V_{mc_1} \quad (\text{VI.1})$$

where V_{mc_1} is the minimum controllable speed airborne in the OEI configuration, that is, the minimum airspeed for straight flight with no more than 5° angle of bank and zero yaw. Minimum climb speed, V_2 , is the climb speed required to clear a 35 foot obstacle and is defined as

$$V_2 = 1.20 V_s \quad (\text{VI.2})$$

[Ref. 8: p. 287]

Take-off profiles can be divided into two types--(1) ground roll to lift-off and climb to clear a 35 foot obstacle; and (2) ground roll to engine failure recognition and abort--as shown in Figure VI.1. These profiles can be broken down into segments as indicated. First, however, a general form of the distance equation must be derived. Since velocity and acceleration, as shown by equation VI.3, are

$$V = \frac{ds}{dt} \text{ and} \tag{VI.3}$$

$$a = \frac{dV}{dt}$$

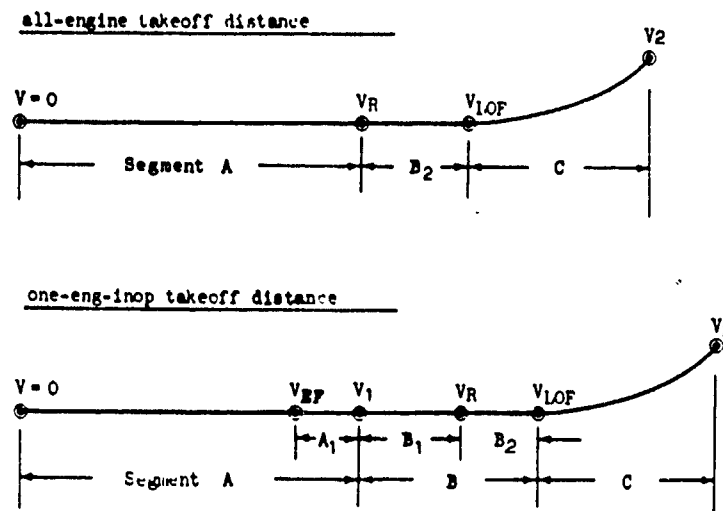


Figure VI.1 Take-off profiles

it follows that distance is

$$ds = \frac{VdV}{a} \tag{VI.4}$$

Integration of equation (VI.4) for the general case of take-off with a constant headwind yields

$$s_G = \int_{V_w}^{V_x} \frac{V - V_w}{a} dV \quad (VI.5)$$

where s_G is the ground roll distance in feet, V_w the surface head wind and V_x any arbitrary speed, both in feet per second. Using Figure (VI.2), which depicts the forces and geometry applicable to the take-off regime, dynamic force equilibrium describing the motion of the aircraft during the ground roll may be written as

$$T - D - \mu(W - L) - W\phi = \frac{W}{g} a \quad (VI.6)$$

or solving for a ,

$$a = \frac{g}{W} [T - \mu W - (D - \mu L) - W\phi] \quad (VI.7)$$

$$a = \frac{g}{W} [T - \mu W - (C_D - \mu C_L)qS - W\phi]$$

where

$$q = \frac{1}{2} \rho V^2 \quad (VI.8)$$

and substituting into equation (VI.5) results in

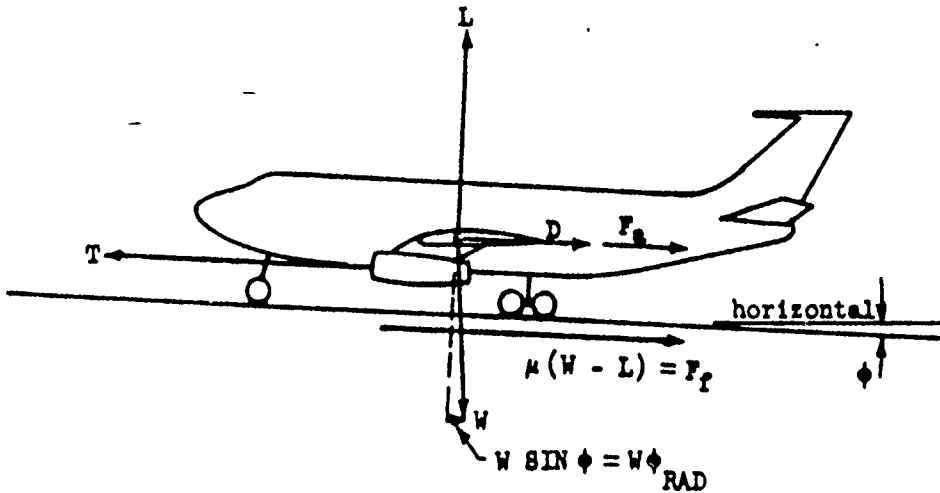


Figure VI.2 Take-off forces

$$s_G = \int_{v_w}^{v_x} \frac{W}{g} \frac{(V - V_w) dV}{[T - \mu W - (C_D - \mu C_L) qS - W \phi]} \quad (\text{VI.9})$$

Some terms within the integrand can be simplified. Lift and drag coefficients can be assumed constant since a tricycle landing gear keeps the aircraft in a constant attitude. Due to the small amount of fuel burned during take-off, weight will be assumed constant (and, in fact, can be made constant in the ACFS by virtue of the fuel freeze mode). However, thrust varies as a function of velocity, temperature and pressure and velocity itself is constantly changing throughout the ground roll. [Ref 7: p. 3.60-3.62]

The problem can be greatly reduced by assuming a constant acceleration, \bar{a} . This average value is defined by examining the relationship between acceleration and the square of velocity which is very nearly linear. For acceleration between zero velocity and

some arbitrary value, V_x , \bar{a} will occur at $(V_x^2)/2$ or $0.707 V_x$. The expression for \bar{a} then becomes equation (VI.7) evaluated at $V = 0.707 V_x$. Rewriting equation (VI.9) gives

$$s_G = \frac{1}{\bar{a}} \int_{V_w}^{V_x} (V - V_w) dV \quad (\text{VI.10})$$

Integration and algebraic simplification yields

$$s_G = \frac{(V_x - V_w)^2}{2\bar{a}} \quad (\text{VI.11})$$

and substituting equation (VI.7) for \bar{a} results in the final form

$$s_G = \frac{(V_x - V_w)^2}{\frac{2g}{W} [T - \mu W - (C_D - \mu C_L) q S - W \phi]} \text{ at } 0.707 V_x \quad (\text{VI.12})$$

If V is expressed in knots then equation (VI.12) becomes

$$s_G = \frac{1.425 (V_x - V_w)^2}{\frac{g}{W} [T - \mu W - (C_D - \mu C_L) q S - W \phi]} \text{ at } 0.707 V_x \quad (\text{VI.13})$$

With reference to Figure VI.1, the length of segment A in the all-engines-operating (AEO) case and segment A up to engine failure speed, V_{LF} , in the one-engine-inoperative (OEI) case can be determined [Ref. 7, p. 3.63-3.66]

Segment A_1 in the OEI case is the distance traveled from actual engine failure to engine failure recognition by the pilot. The velocity change is

$$\Delta V = \frac{\Delta t(\bar{a})}{1.688} \quad (\text{VI.14})$$

where \bar{a} is given by

$$\bar{a} = \frac{g}{W} \left(T\bar{\eta} - \mu W - (C_D - \mu C_L) S \frac{V^2 \sigma}{295.37} - W\phi \right) \quad (\text{VI.15})$$

The $\bar{\eta}$ term is the ratio of the average thrust across this period to the AEO thrust at V_1 . Substituting into equation (VI.14) yields a form of the velocity difference which may be iterated to find V_1 for assumed values of V_{EF} .

$$V_{EF} = V_1 - \frac{\Delta t g}{1.688} \left[\bar{\eta} \left(\frac{T}{W} \right) - \mu - (C_D - \mu C_L) \frac{S V_1^2 \sigma}{295.37 W} - \phi \right] \quad (\text{VI.16})$$

Since the time span across A_1 is typically on the order of two or three seconds, the distance covered can be closely approximated by the first form of equation (VI.3) rewritten as

$$\Delta s = V \Delta t \quad (\text{VI.17})$$

This distance is typically small in comparison to the actual take-off distance and so the change in velocity across it is not great. The velocity can be approximated by the average velocity between $V_{L.F.}$ and V_1 . Performing this substitution and integrating equation (VI.17) gives

$$s_{A_1} = 1.688 \left(\frac{V_1 + V_{EF}}{2} - V_w \right) \Delta t \quad (VI.18)$$

where Δt is the time from engine failure to recognition.[Ref. 7: p. 3.73]

Segment B_1 is the distance in the OEI case from engine failure recognition to rotation speed, V_R . This distance can be found through the use of equation (VI.9). Thrust will be assumed to be the average thrust across the entire OEI ground roll from engine failure to rotation. Dynamic pressure, q , is also a function of velocity so the expression $V^2 \rho_0 \sigma / 2$ is substituted and the integration performed yielding

$$s_{B_1} = \frac{W}{2g} \left[-\frac{1}{a} \ln(aV^2 + c) - \frac{V_w}{\sqrt{-ac}} \ln \frac{\sqrt{c} + V\sqrt{-a}}{\sqrt{c} - V\sqrt{-a}} \right]_{V_1}^{V_R} \quad (VI.19)$$

where

$$\begin{aligned} a &= -(C_D - \mu C_L) \frac{1}{2} \rho_0 \sigma \\ c &= T - \mu W - W \phi \end{aligned} \quad (VI.20)$$

Segment B_2 (for both the OEI and AEO cases) can be calculated in the same manner as that for Segment A_1 by substituting V_R for V_1 and V_1 for V_{EF} . Similarly, Segment C for both cases can be found using the average velocity between V_R and V_{LOF} . [Ref. 7: p. 3.73-3.74]

For the OEI case in which a pilot initiates a take-off abort two additional distances must be calculated. The first, Segment D, is the transition distance or distance from engine failure recognition to achievement of the full braking configuration, that is, brake application, spoiler deployment and idle thrust at V_{sp} . The second, Segment E, is the distance from V_{sp} to a full stop, or stopping distance.

A velocity change, $\Delta V = V_{sp} - V_1$, occurs across the transition distance which can be represented by

$$\Delta V = \frac{(\Delta t)\bar{a}}{1.688} \quad (\text{VI.21})$$

since V_{sp} is unknown. Equation (VI.7) can be used to calculate \bar{a} from conditions at V_1 with little error. The thrust term will be the average thrust across this distance. The length of Segment D can now be determined by using an analogy to equation (VI.18)

$$s_D = 1.688 \left(V_1 + \frac{\Delta V}{2} - V_w \right) \Delta t \quad (\text{VI.22})$$

[Ref. 7: p. 3.74-3.75]

Stopping distance is found by integrating equation (VI.9) from V_{sp} to V_w . Again, the dynamic pressure term must be expressed as a function of velocity resulting in equations (VI.19) and (VI.20). All terms in equations (VI.20) are constant with respect to the braking phase (i.e., idle thrust, drag and lift changes due to spoiler employment, and braking friction coefficient).[Ref. 7: p. 3.75-3.76]

Balanced field length is defined as the length required to accelerate to engine failure recognition speed, continue to lift-off and clear a 35 foot obstacle or abort the take-off with maximum braking effort. Figure VI.3 shows that by assuming several different engine failure speeds the sums $B+C$ and $D+E$ can be plotted against V_1 with the point of intersection giving the conditions for balanced field length. Since Segment A has the same value for both cases, adding A to this distance results in the balanced field length. The engine failure speed, V_{EF} , corresponding to this particular case then becomes the critical engine failure speed and the engine failure recognition speed, V_1 , the decision speed.[Ref. 7; p. 3.76-3.77, Ref. 8: p. 286]

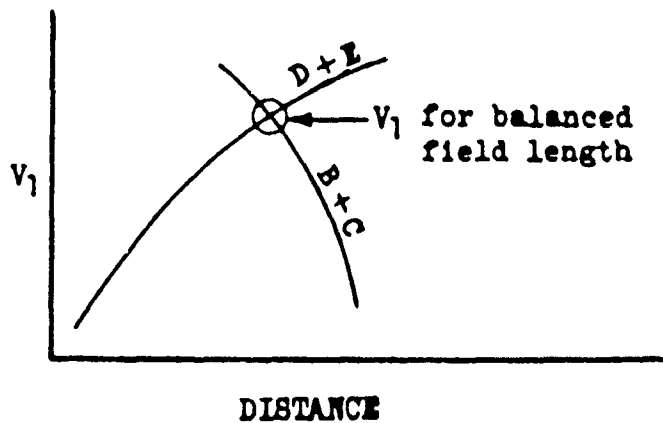


Figure VI.3 Graphical determination of balanced field length and decision speed

B. FLIGHT TEST PROCEDURES

1. Climb speed

Climb speed is related to stall speed through equation (VI.2); therefore the procedures used in finding stall speeds were applicable and the data presented in Chapter V.C for the take-off configuration were used.

2. Airborne minimum control speed

The airborne minimum control speed was found by performing an OEI stall series in the take-off configuration. The ACFS was flown at 200 feet AGL to ensure the aircraft was out of ground effect. Gross weights from 150,000 to 220,000 pounds were examined. The following parameters were monitored and recorded via the GCU page.

- Calibrated airspeed
- Gross weight
- Altitude
- Thrust
- Bank angle
- Lift coefficient due to ground effect

3. Decision speed/Balanced field length

Data were collected by performing take-off ground rolls corresponding to rotation and lift-off speeds as functions of gross weight. Head wind and runway slope were both assumed as zero which greatly simplified some of the equations and integral

expressions previously developed. Several engine failure speeds were assumed for each gross weight and test runs conducted for each in the following manner.

The AEO condition was tested first. The simulator was placed at rest on the runway and the throttles advanced to the maximum take-off position. At 70.7% of the precalculated lift-off speed the simulator was frozen and data recorded. This routine was completed for all temperature/gross weight combinations. The next set of test runs dealt with the OEI environment and was carried out in the following fashion. An engine failure speed, V_{EF} , was assumed prior to each run. The aircraft was accelerated to this speed, one engine retarded to idle, and the simulator frozen for data recording. The simulator was put back on line for two seconds, to approximate the delay during which the pilot recognizes engine failure, and frozen again to obtain data at this assumed V_1 . The simulator was then allowed to complete the take-off run to V_R where the final set of data was recorded. Using the data recorded along with the assumed V_{EF} values an iteration of equation (VI.15) was performed to compute the actual V_1 . Lastly, abort test runs were conducted by accelerating to V_1 and simultaneously reducing both throttles to idle, deploying the spoilers and applying maximum brake pressure. The simulator was then frozen and a data set recorded.

C. FLIGHT TEST RESULTS

Table VI.1 shows the balanced field lengths required for the ACFS for several gross weights and an OAT of 10°C at sea level. The field lengths increased with increasing gross weight as expected. Table VI.2 is a comparison of the critical take-off speeds (V_1 ,

V_{K} , V_2) of the ACFS and Boeing 757 and 767 at sea level for an OAT of 10°C. The 767 data represented the lower limit of aircraft gross weight. Combined with more powerful engines this resulted in considerably lower speeds in all cases for the same gross weight. The ACFS showed an improving trend toward lower decision and rotation speeds indicating shorter take-off ground roll distances. Climb speed was slightly higher than the 757, however, giving rise to a considerable gap between rotation and climb speeds. This may be attributable to the assumptions made in developing the theory for this test. Climb speed was calculated as a minimum value to represent the most critical scenario and, thus, cannot be reduced further. Rotation speed was also calculated as a minimum as per Reference 6. Because of limited simulator availability these values were not tested to determine if acceptable rotation rates were possible.

TABLE VI.1 ACFS balanced field length

GROSS WEIGHT (LB)	160000	180000	200000	220000
BALANCED FIELD LENGTH (FT)	2901	3440	4221	5144

TABLE VI.2 Comparison of critical take-off speeds

GROSS WT (1000 LB)	AIRCRAFT TYPE									
	757 (20° FLAPS)			767 (20° FLAPS)			ACFS (40° FLAPS)			V ₂
	V ₁	V _R	V ₂	V ₁	V _R	V ₂	V ₁	V _R	V ₂	
220	133	136	140	108	110	120	116	119	144	
200	125	128	133	102	103	114	111	116	135	
180	117	120	126	NOT AVAILABLE			107	109	127	
160	108	112	119	NOT AVAILABLE			101	104	122	
AIRPORT ELEVATION: SEA LEVEL OAT: 10°C										

VII. CONCLUSIONS AND RECOMMENDATIONS

A. CONCLUSIONS

The results obtained in this study represent a solid base for further development of the ACFS in terms of its aerodynamic performance. The Boeing 757 and 767 aircraft were used as relative measures of the accuracy of the predictions of mid-1990's technology. These aircraft represent the state-of-the-art in commercial transports of the same relative size as the ACFS as shown in Figure I.1.

A review of the maximum EPR flight test results showed the ACFS to have considerably higher EPR values than both the 757 and 767 in the terminal phases of flight (i.e., take-off and landing). However, in the higher altitude (climb) regime the ACFS had either slightly higher or lower values. Given the improvements in EPR performance between the 757 and 767, the ACFS was expected to outperform both aircraft in all measures of EPR performance. The inconsistent performance of the ACFS in the climb phase indicated the existence of a software logic error in one or both of two EPR criteria. The first area is any relationship involving both altitude and PLA. Since the EPR values were between those of the two Boeing aircraft at low altitudes and higher than both aircraft at high altitudes without changing PLA, an invalid logic condition at altitudes of 15,000 feet and below was suspected to exist. The second possible area of concern is the

source of ACFS EPR values (algorithm or look-up table). An error in this area would cause incorrect EPR values to be used despite all logic conditions being properly satisfied.

Comparison of the ACFS optimum long range cruise Mach numbers with those of the Boeing 757 showed the ACFS to have consistently lower values indicating the ACFS drag divergence Mach number to be considerably lower than that of the 757. Higher values of M_{dd} benefit airliners by allowing for faster cruise speeds without high drag penalties. Most commercial transport aircraft have been designed so as to delay the onset of drag divergence at high altitudes (35,000-40,000 feet) until approximately $M=0.8-0.85$, prior to the onset of transonic flow. The ACFS optimum cruise did not occur at these typical values indicating an inconsistency in the influence of drag divergence upon the aerodynamic model. Though, when viewed in terms of wing loading and lift coefficient, the results were qualified. The ACFS actually cruised at equal or higher lift coefficients than the 757.

The results of the flap reference speed testing revealed the ACFS required at least ten knots of additional airspeed above that required for the 757 to avoid stalling. Once again, due to the difference in wing loadings the results were examined in terms of lift coefficient. The ACFS was found to have consistently lower maximum lift coefficients at the 27° flap setting than the 757 did at 25° flaps by a factor of 20%-25%. This led to the conclusion that a deficiency existed in the ACFS aerodynamic model in terms of maximum lift coefficient.

The critical take-off and balanced field length testing showed the ACFS required lower velocities than the 757 for comparable gross weights. Again, the 767 gross weights

were at the low end of that aircraft's weight spectrum which explains the lower velocities. The climb speeds for the ACFS were considerably higher due to the approximation method used. However, this is a conservative estimation resulting in longer balanced field lengths than actually necessary. Balanced field length data for the Boeing aircraft were unavailable for comparison.

B. RECOMMENDATIONS

The following courses of action are recommended in order to further investigate possible deficiencies in the ACFS.

- Examine the software logic governing the calculation of EPR while in the climb phase. Ensure the source of EPR values (algorithm or look-up table) is accurate.
- Examine the aerodynamic modelling software to determine the validity of drag divergence calculations.
- Examine lift augmentation modelling to refine maximum lift coefficient and lower stall speeds. The apparent low maximum C_L values may have been due to the computer limit on control inputs when approaching a stall condition.
- Determine the feasibility of creating an airborne reinitialization feature for the simulator. This would be especially helpful when performing multiple approaches to landing during software development or further performance evaluations.
- Future follow-on work to this research would be better served by using a different aircraft for comparison in place of the Boeing 767. The Airbus A320 is recommended as a substitute.
- Time histograms may prove useful in future research but are presently difficult due to the nature of time variables present in the ACFS software. If histograms are desired use of videotape, if feasible, is recommended.

APPENDIX

TABLE A.1 ACFS Take-off EPR

OAT (°C)	AIRPORT PRESSURE ALTITUDE (1000 FT)								
	SL	1	2	3	4	5	6	7	8
70	1.30	1.30	1.31	1.31	1.31	1.32	1.32	1.32	1.32
65	1.32	1.32	1.32	1.33	1.33	1.34	1.34	1.34	1.33
60	1.33	1.34	1.34	1.35	1.35	1.36	1.36	1.36	1.36
55	1.35	1.36	1.36	1.37	1.37	1.38	1.38	1.38	1.38
50	1.38	1.38	1.39	1.39	1.40	1.40	1.40	1.40	1.40
45	1.40	1.41	1.41	1.42	1.42	1.43	1.43	1.43	1.43
40	1.43	1.43	1.44	1.44	1.45	1.46	1.46	1.45	1.45
35	1.45	1.46	1.47	1.47	1.48	1.49	1.48	1.48	1.48
30	1.48	1.49	1.50	1.50	1.51	1.52	1.52	1.52	1.51
25	1.48	1.50	1.52	1.53	1.54	1.55	1.55	1.55	1.55
20	1.48	1.50	1.52	1.54	1.56	1.58	1.58	1.58	1.58
15	1.48	1.50	1.52	1.54	1.56	1.58	1.60	1.61	1.62
10	1.48	1.50	1.52	1.54	1.56	1.58	1.60	1.61	1.63

TABLE A.2 ACFS Climb EPR

TAT (°C)	PRESSURE ALTITUDE 1000 FT								
	0	5	10	15	20	25	30	35	40
60	1.19	1.17	1.16	1.15	1.16	1.15	1.19	****	****
50	1.23	1.22	1.20	1.19	1.19	1.17	1.20	1.19	****
40	1.26	1.25	1.24	1.23	1.22	1.21	1.22	1.21	****
30	1.29	1.30	1.28	1.28	1.27	1.26	1.23	1.24	1.26
20	1.28	1.32	1.34	1.35	1.33	1.32	1.29	1.31	1.30
10	1.29	1.32	1.37	1.39	1.39	1.39	1.37	1.37	1.36
0	1.28	1.32	1.37	1.39	1.43	1.48	1.45	1.43	1.44
-10	1.28	1.31	1.37	1.39	1.42	1.47	1.52	1.53	1.52
-20	1.28	1.31	1.37	1.39	1.42	1.46	1.51	1.61	1.61

TABLE A.3 ACFS Go-around EPR

OAT (°C)	AIRPORT PRESSURE ALTITUDE (FT)							
	0	1000	2000	3000	4000	5000	6000	8000
55	1.35	1.35	1.36	1.38	1.37	1.38	1.38	1.38
50	1.36	1.37	1.39	1.39	1.40	1.40	1.40	1.40
45	1.39	1.40	1.41	1.42	1.42	1.44	1.43	1.43
40	1.42	1.42	1.44	1.46	1.45	1.46	1.46	1.46
35	1.44	1.46	1.47	1.49	1.49	1.49	1.48	1.48
30	1.47	1.48	1.50	1.50	1.52	1.53	1.53	1.53
25	1.47	1.50	1.53	1.55	1.56	1.56	1.57	1.56
20	1.48	1.49	1.53	1.57	1.57	1.60	1.60	1.60
15	1.48	1.49	1.53	1.55	1.57	1.59	1.62	1.63
10	1.46	1.50	1.52	1.56	1.58	1.59	1.61	1.65

TABLE A.4 ACFS Long range cruise Mach numbers

GROSS WEIGHT (LB)	ALTITUDE (FT)			
	25000	30000	35000	40000
200000	0.66	0.71	0.73	0.75
180000	0.66	0.69	0.72	0.74
160000	0.60	0.65	0.71	0.72

TABLE A.5 ACFS Critical take-off speeds

GROSS WT (1000 LB)	TAKE-OFF VELOCITIES (KCAS)		
	V₁	V_R	V₂
220	116	119	144
200	111	116	135
180	107	109	127
160	101	104	122

AIRPORT ELEVATION: SEA LEVEL OAT: 10°C

LIST OF REFERENCES

1. The Boeing Company, *Boeing 757 Operations Manual*, 10 December 1982.
2. The Boeing Company, *Boeing 767 Operations Manual*, 1 November 1983.
3. Taylor, John W. R., ed., *Jane's All the World's Aircraft 1989-90*, Alexandria, VA, Jane's Information Group, 1990.
4. Donohue, Paul F., *An Aerodynamic Performance Evaluation of the NASA/Ames Research Center Advanced Concepts Flight Simulator*, Master's Thesis, Naval Postgraduate School, Monterey, California, June 1987.
5. National Aeronautics and Space Administration Contractor Report 166068, *Crew Systems and Flight Station Concepts for a 1995 Transport Aircraft*, by George A. Sexton, April 1983.
6. National Aeronautics and Space Administration Software Description 7005, *Software Description (SD) Document for the ACFS Computer Upgrade*, by NSI Technology Services Corporation, 16 October 1989.
7. The Boeing Company, *Jet Transport Performance Methods*, Sixth Edition, May 1969.
8. Shevell, Richard Shephera, *Fundamentals of Flight*, Prentice-Hall, Inc., 1983.

INITIAL DISTRIBUTION LIST

1. Defense Technical Information Center 2
Cameron Station
Alexandria, VA 22304-6145
2. Library, Code 52 2
Naval Postgraduate School
Monterey, CA 93943-5002
3. Professor E. Roberts Wood, Code AA/Wd 1
Chairman,
Department of Aeronautics and Astronautics
Naval Postgraduate School
Monterey, CA 93943-5000
4. Professor Max Platzler, Code AA/Pl 1
Director,
Navy-NASA Joint Institute of Aeronautics
Naval Postgraduate School
Monterey, CA 93943-5000
5. Professor Louis V. Schmidt, Code AA/Sc 1
Department of Aeronautics and Astronautics
Naval Postgraduate School
Monterey, CA 93943-5000
6. Professor Richard M. Howard, Code AA/Ho 1
Department of Aeronautics and Astronautics
Naval Postgraduate School
Monterey, CA 93943-5000
7. Robert J. Shiner 5
Director, Man-Vehicle Systems Research Facility
NASA/Ames Research Center (Mail Stop 257-1)
Moffett Field, CA 94035
8. LT Thomas P. McKavitt, Jr., USN 2
Carrier Air Wing Fourteen (CVW-14)
FPO San Francisco, CA 96601-4409